Electronic Supplementary Material (ESI) for Energy & Environmental Science.

Supporting Information

Increasing Stability, Efficiency, and Fundamental Understanding of Lithium-Mediated Electrochemical Nitrogen Reduction

Suzanne Z. Andersen[a†], Michael J. Statt[b†], Vanessa J. Bukas[a†], Sarah G. Shapel[a], Jakob B. Pedersen[a], Kevin Krempl[a], Mattia Saccoccio[a], Debasish Chakraborty[a], Jakob Kibsgaard[a], Peter C. K. Vesborg[a], Jens Nørskov[a*], and Ib Chorkendorff[a*]

[a.] *Department of Physics, Technical University of Denmark, Kongens Lyngby, Denmark.*
[b.] *SUNCAT Center for Interface Science and Catalysis, Department of Chemical Engineering, Stanford University, Stanford, CA, USA*
[c.] ** Corresponding author emails: jkno@dtu.dk ibchork@fysik.dtu.dk*
[d.] *† These authors have contributed equally*

Electrochemical experiments

Measurements are done in a 3-electrode single compartment glass cell enclosed in an electrochemical autoclave, placed in a fumehood. Electrolyte solution consisting of 0.3 M $LiClO_4$ (Battery grade, dry, 99.99 %, Sigma Aldrich) in 99 vol. % tetrahydrofuran (THF, anhydrous, >99.9 %, inhibitor-free, Sigma Aldrich) and 1 vol.% ethanol (EtOH, anhydrous, Honeywell) was prepared in an Ar glovebox. The electrolyte is pre-saturated with purified (SAES Pure Gas, MicroTorr MC1-902F) N_2 (5.0, Air Liquide) gas for 1-2 hours at approximately 5 mL/min, in a sealed glass cell in the glovebox. This gas cleaning is done to avoid any ammonia or labile nitrogen containing contaminants in the gas itself (*1*, *2*). Roughly, 35-40 p.p.m. of water contamination is measured in the pre-saturated electrolyte via Karl Fischer Titration (831 KF Coulometer and 728 Stirrer, Metrohm). The working electrode (WE) is a Mo foil (+99.9 %, Goodfellow) spot-welded with Mo wire (99.85 %, Goodfellow) for good electrical connection. Prior to electrochemical tests, the WE is dipped in 2 wt.% HCl (VWR Chemicals) to dissolve any surface species of Li, and rinsed in ultra-pure water (18.2 MΩ resistivity, Millipore, Synergy UV system) and EtOH. The WE is polished using Si-C paper (Buehler, CarbiMet P1200), and again rinsed thoroughly in EtOH. The counter electrode (CE) consists of a Pt mesh (99.9 %, Goodfellow), and the reference electrode (RE) is a Pt wire (99.99 %, Goodfellow). The CE and RE are both boiled in ultra-pure water, and dried overnight at 100 ^oC, then flame-annealed. The single compartment glass cell and a magnetic stirring bar (VWR, glass covered) is boiled in ultra-pure water, and dried overnight at 100 ^oC in air. The WE and CE are ~0.5 cm apart, and the surface area of the WE facing the CE is 1.8 cm^2. Prior to an electrochemical experiment, we introduce Ar gas (5.0, Air Liquide) into the empty assembled cell placed in the autoclave for 1 hour. The denser Ar gas substantially displaces the atmospheric laboratory air, mainly consisting of N_2 and O_2, in the system, as measured via mass spectrometry. Next, we inject electrolyte solution into the cell in Ar atmosphere, and the autoclave is closed. Finally, the pressure is increased to 10 bar with either N_2 or Ar depending on the intended experiment, and de-pressurized to 3 bar a total of 9 times, in order to flush out any remaining atmospheric contaminants, then filled to 10 bar. Subsequently, the electrochemical experiments, including potentiostatic electrochemical impedance spectroscopy (PEIS) to determine the resistance in our cell, with 85 % manual *iR*-drop correction, a linear sweep voltammetry (LSV) from open circuit voltage (OCV) until lithium reduction is clearly seen, then chronopotentiometry (CP), followed by another impedance measurement to ensure that the resistance has not changed, are started. We determine the lithium reduction potential scale based on the LSV. The onset for lithium reduction is quite clear, and we can thereby denote the potential *vs* Li^+/Li. During CP, either a steady current density of -2 mA/cm^2 is used (hereafter denoted deposition potential), or a cyclic method with -2 mA/cm^2 for 1 min, followed by 0 mA/cm^2 (hereafter denoted resting potential) for 3-8 min, depending on whether the WE potential needed to be increased, decreased, or stabilized. We note that all experiments were conducted at room temperature. A slightly elevated temperature of 50 ^oC suggests drastic change in the electrolyte composition due to decomposition or other side- reaction(s) that changed the electrolyte color to yellow.

Gas chromatography-mass spectrometry (GC-MS) measurements before and after the experiments show an expected decrease in the concentration of the sacrificial EtOH, and appearance of a new peak assigned to the newly formed NH_3. When operating within a regime where the EtOH proton source was significantly depleted (<0.75 vol.%), we have detected trace amounts of dihydrofuran which is a THF oxidation product. This regime is avoided in the experiments presented in this study by increasing the initial EtOH concentration for longer measurements (to e.g. 2 vol.% for 125 hour operation).

Colorimetric quantification of ammonia

Synthesized ammonia was quantified by a modified colorimetric indophenol method (*3*), previously described (*1*). The sample absorbance was analyzed by UV/Vis spectroscopy (UV-2600, Shimadzu) in the range from 400 nm to 1000 nm. The blank solution is subtracted from each spectrum, and the difference between the peak around 630 nm and the trough at around 850 nm is used. A fitted curve of the difference between the peak and trough of each concentration showed a linear regression with an R^2 value of 0.998. We utilize this method, as

opposed to the more common peak based method, because long experiments might have solvent breakdown, which can give a falsely high peak at the ammonia wavelength, due to interference from the evolved solvent background. The amount of ammonia in the headspace was quantified by de-gassing the system through an ultra-pure water trap. For each measurement, a 0.5 mL sample of the water trap was taken, and four 0.5 mL samples were taken from the electrolyte. One sample from the electrolyte is used as a background, and the mean and standard deviation of the remaining 3 samples is reported in Table S1. The remaining samples were treated as described previously (*1*), to determine the ammonia concentration. If the expected concentration of ammonia exceeds the concentration limits of the indophenol method, the sample is accordingly diluted with ultra-pure water after drying.

Control experiments

To perform an Ar blank experiment, the electrolyte was pre-saturated with Ar instead of N_2, and after injection into the autoclave cell, the pumping and purging procedure was carried out with Ar instead of N_2. An electrochemical cycling experiment with -2 mA/cm^2 for 1 min followed by 0 mA/cm^2 for 3-4 minutes was carried out, with a 3 hour rest at 0 mA/cm^2 after around 15 hours, to allow full diffusion of any potential ammonia in solution. Additionally, ammonia contamination in blank measurements at OCV for 24 hours at 10 bar N_2, were also performed.

Isotope sensitive quantification of $^{15}NH_3$ and $^{14}NH_3$

For the isotopically labelled nitrogen measurement, a mass spectrometer (Pfeiffer, OmniStar GSD 320) was connected to the autoclave, to determine the supplied ratio of $^{15}N_2$ to $^{14}N_2$ gas. The total internal autoclave volume is approximately 380 mL at STP, and around 320 mL of gas volume at STP with the electrochemical cell inside. After air displacement with Ar, the pressure in the autoclave was raised to 10 bar and purged to 3 bar a total of 9 times with $^{14}N_2$, then the $^{15}N_2$ gas was added up to 5 bar, and lastly the $^{14}N_2$ gas again up to 10 bar. The relative ratio measured via mass spectrometry was 78 ± 2 % $^{14}N_2$ and 22 ± 2 % $^{15}N_2$ supplied to the system. Two additional 0.5 mL samples from the electrolyte are taken after electrolysis, and one of them is diluted 5:1 to fall in the appropriate range of the calibration curve previously made. The samples are then treated according to the previously published protocols to quantitatively determine the isotope concentration of the produced ammonia via NMR (*1*, *4*), where the undiluted sample is used to ensure the desired ratio of 1:5 from the dilution step.

Ex-situ electrode characterization

After electrochemistry, the samples were characterized with several different techniques. It should be noted that the samples were exposed to air, and the composition is therefore not representative of in-operando measurement conditions. Scanning Electron Microscopy (SEM) images were taken with a Quanta FEG 250 SEM from FEI, equipped with an Oxford Instruments 80 mm^2 X-Max silicon drift EDX detector for elemental mapping. The morphology of the samples shown in Figure 3 was recorded with an ETD detector for secondary electrons at various electron energies and magnifications, specified in each image shown in Figure S1-2. Energy Dispersive X-ray (EDX) quantification was done with AZtec software from Oxford Instruments. X-ray Diffraction (XRD) was recorded with a Malvern PANanalytical Empyrean X-ray diffractometer, equipped with parallel beam optics and a parallel plate collimator of 0.18°. The source is an Empyrean Cu LFF HR gun operated at 45 kV and 40 mA, with Kα = 1.540598 Å. Grazing-incidence geometry was used to minimize the contribution of the substrate, i.e. the Mo foil, with an incident radiation beam fixed at a grazing angle of 0.4°. X-ray Photoelectron Spectroscopy (XPS) was done using a ThermoScientific Thetaprobe instrument equipped with an Al K_α X-ray source. Survey spectra were recorded with 20 scans at 50 ms dwell time per 1 eV step. Elemental detail spectra were recorded with 5-50 scans in 0.1 eV steps with 50 ms dwell time. The chamber pressure was $2 \cdot 10^{-7}$ mbar, and the lateral resolution was 400 µm. A Flood Gun in Charge Neutralization mode was used during the measurement. The data was acquired and analyzed using Thermo Advantage v5.979 by Thermo Fischer Scientific.

Efficiency calculations

To calculate the Faradaic efficiency (FE), the concentration, C_{NH3}, of synthesized ammonia in the electrolyte is measured via either a colorimetric or isotope sensitive method, along with the total electrolyte volume, *V*, after each measurement. This is compared with the total charged passed, *Q*:

$$\boldsymbol{FE_{NH3} = \frac{3 \cdot F \cdot C_{NH3} \cdot V}{Q}}$$

where *F* is Faraday's constant, and 3 is the number of electrons transferred during the reaction for each mole of NH_3.

To estimate the energy efficiency, η, we considered the total amount of energy put into the system via the potentiostat, E_{in}, and compared that to the energy contained in the total amount of ammonia produced during the experiment, E_{out}.

$$\boldsymbol{\eta = \frac{E_{out}}{E_{in}}}$$

We define E_{out} by the free energy of reaction of ammonia oxidation to N_2 and water times the amount of ammonia produced, while E_{in} is given by the total cell voltage between the counter electrode (CE) and working electrode (WE), multiplied by the current to get the instantaneous power, and integrated over time:

$$\boldsymbol{E_{out} = \Delta G_r \cdot m_{NH3}}$$

$$\boldsymbol{E_{in} = \int (V_{CE}(t) - U(t)) \cdot I(t)\, dt}$$

Unlike the reported voltages, the voltage used to calculate the energy efficiency is not *iR*-corrected, and the resistance-related losses thus result in a decreased total calculated energy efficiency.

Proposed Cycling Mechanism

As described in the main text, the mechanism we propose for ammonia production during the periods of no applied potential utilizes an electron stored in reduced lithium to produce either ammonia or hydrogen. As this electron is held at the reduction potential of Li^+, the assumptions regarding the speed of electrochemical reactions should be unaffected leaving both HER and eNRR limited by the rate of diffusion of either protons or nitrogen. The proportion of lithium used to run steps 3(b-e) below is what is denoted as $\boldsymbol{s_{Li \to NH_3}}$ in Equation (7) and (8).

$$H^+ \underbrace{\overset{r_H}{\rightarrow}}_{slow} H^+_{(s)} \qquad \text{(2a-cycle)}$$

$$N_2 \underbrace{\overset{r_{N_2}}{\rightarrow}}_{slow} N_{2(s)} \qquad \text{(3a-cycle)}$$

$$Li\cdot + \left(H^+_{(s)} + Li\cdot\right) \underbrace{\xrightarrow{k^{cycle}_{H-1}}}_{fast} Li \cdot H^* \qquad \text{(2b-cycle)}$$

$$Li \cdot H^* + \left(H^+_{(s)} + Li\cdot\right) \underbrace{\xrightarrow{k^{cycle}_{H-2}}}_{fast} Li\cdot + H_2 \qquad \text{(2c-cycle)}$$

$$Li\cdot + {}^1\!/_2\, N_{2(s)} \underbrace{\xrightarrow{k^{cycle}_{N-1}}}_{fast} Li \cdot N^* \qquad \text{(3b-cycle)}$$

$$Li \cdot N^* + \left(H^+_{(s)} + Li\cdot\right) \underbrace{\xrightarrow{k^{cycle}_{N-2}}}_{fast} Li \cdot NH^* \qquad \text{(3c-cycle)}$$

$$Li \cdot NH^* + \left(H^+_{(s)} + Li\cdot\right) \underbrace{\xrightarrow{k_{N-3}^{cycle}}}_{fast} Li \cdot NH_2^* \qquad \text{(3d-cycle)}$$

$$Li \cdot NH_2^* + \left(H^+_{(s)} + Li\cdot\right) \underbrace{\xrightarrow{k_{N-4}^{cycle}}}_{fast} Li \cdot + NH_3 \qquad \text{(3e-cycle)}$$

Reduced lithium may also reduce solvent species by donating its electron to them as it dissolves. This would represent a lost electron similar to any electron used to run HER, decreasing $\boldsymbol{s_{Li\rightarrow NH_3}}$.

Kinetic Model Fitting

To connect experimental conditions to values of r_{N_2}/r_{Li} and r_H/r_{Li} we fit 3 parameter model to experimental values of FE. During fitting, $\mathrm{P_{N_2}}$ and $\mathrm{C_{EtOH}}$ are assumed to be directly proportional to r_{N_2}/r_{Li} and r_H/r_{Li}, respectively. As a result, we utilize two fitted conversion factors to relate P_{N_2} to r_{N_2}/r_{Li} and $\mathrm{C_{EtOH}}$ to r_H/r_{Li}:

$$r_{N_2}/r_{Li} = A_{N_2}P_{N_2} \qquad \text{(9a)}$$

$$r_H/r_{Li} = A_{EtOH}C_{EtOH} \qquad \text{(9b)}$$

These two conversion factors, along with $s_{Li\rightarrow NH_3}$, are treated as free parameters in the model. The values are fit to the experimental values of FE shown in Table S1. Equation (8) is used for cycling data points and Equation (6) is used for constant deposition data points. Least squared error is minimized using the scipy optimization library in python. The resultant values for the three parameters is shown below:

Parameter	Fit Value
A_{N_2}	0.0055 bar^{-1}
A_{EtOH}	0.31 $\mathrm{vol\%}^{-1}$
$s_{Li\rightarrow NH_3}$	0.18

The overall root mean squared error and r^2 for the fitted model was 2.84% and 0.94, respectively. As r_{N_2}/r_{Li} and r_H/r_{Li} can be mapped directly to nitrogen pressure and ethanol concentration we can make versions of Figures 2 and 3 with the axes replaced by these experimental conditions, as shown in Figures S14 and S15. In Figure 3(a) and S15(a), constant values for r_H/r_{Li}=0.33 which corresponds to a C_{EtOH}=1 vol% prior to conversion using A_{EtOH} above. Similarly, r_{N_2}/r_{Li} was held constant at a value of 0.055 in Figures 3(b) and S15(b), which corresponds to $P_{N_2} = 10$ bar.

References

1. S. Z. Andersen, V. Čolić, S. Yang, J. A. Schwalbe, A. C. Nielander, J. M. McEnaney, K. Enemark-Rasmussen, J. G. Baker, A. R. Singh, B. A. Rohr, M. J. Statt, S. J. Blair, S. Mezzavilla, J. Kibsgaard, P. C. K. Vesborg, M. Cargnello, S. F. Bent, T. F. Jaramillo, I. E. L. Stephens, J. K. Nørskov, I. Chorkendorff, A rigorous electrochemical ammonia synthesis protocol with quantitative isotope measurements. *Nature*. **570**, 504–508 (2019).
2. R. Dabundo, M. F. Lehmann, L. Treibergs, C. R. Tobias, M. A. Altabet, P. H. Moisander, J. Granger, The Contamination of Commercial 15N2 Gas Stocks with 15N–Labeled Nitrate and Ammonium and Consequences for Nitrogen Fixation Measurements. *PLoS One*. **9**, e110335 (2014).
3. P. L. Searle, The berthelot or indophenol reaction and its use in the analytical chemistry of nitrogen. A review. *Analyst*. **109**, 549 (1984).
4. A. C. Nielander, J. M. McEnaney, J. A. Schwalbe, J. G. Baker, S. J. Blair, L. Wang, J. G. Pelton, S. Z. Andersen, K. Enemark-Rasmussen, V. Čolić, S. Yang, S. F. Bent, M. Cargnello, J. Kibsgaard, P. C. K.

Vesborg, I. Chorkendorff, T. F. Jaramillo, A Versatile Method for Ammonia Detection in a Range of Relevant Electrolytes via Direct Nuclear Magnetic Resonance Techniques. *ACS Catal.* **9**, 5797–5802 (2019).

5. D. D. Wagman, W. H. Evans, V. B. Parker, R. H. Schumm, I. Halow, S. M. Bailey, K. L. Churney, R. L. Nuttall, The NBS tables of chemical thermodynamic properties. Selected values for inorganic and C1 and C2 organic substances in SI units [J. Phys. Chem. Ref. Data 11, Suppl. 2 (1982)]. *J. Phys. Chem. Ref. Data*. **18**, 1807–1812 (1989).

Sample name	FE (%)	Charge (C)	NH_3 (μg)	NH_3 Conc. (p.p.m.)	Vol. (mL)	Energy efficiency (%)
Constant 1 (IP)	20.2 ± 1.0	27.4	325 ± 16	10.0 ± 0.5	32.5	1.8 ± 0.1
Constant 2 (IP)	21.3 ± 1.2	21.4	267 ± 15	9.4 ± 0.5	28.5	2.2 ± 0.2
Constant 3 (IP)	21.4 ± 0.5	23.3	293 ± 6	11.0 ± 0.2	26.7	2.8 ± 0.1
Cycling 1 (IP)	36.4 ± 0.4	100.0	2143 ± 22	72.6 ± 0.7	29.5	7.5 ± 0.1
Cycling 2 (IP)	37.2 ± 1.2	100.0	2188 ± 70	53.7 ± 1.9	37.8	6.8 ± 0.2
Cycling 3 (Isotope, IP)	37.6 ± 2.0	100.0	2212 ± 114	81.3 ± 4.2	27.2	6.5 ± 0.4
Cycling 3 (NMR: $^{15}NH_3/^{14}NH_3$)	38.2	100.0	423 / 1823	15.6 / 67.1	27.2	6.6

Table S1 All measured values for each indophenol experiment reported at 10 bar N_2 with 1 % EtOH. The mean and standard deviation stems from measured absorbance of 3 electrolyte samples from each measurement. Sample designated with numbers are repeated measurements under the same conditions. Cycling 3 is an experiment with isotope labelled N_2, measured with indophenol (IP) and NMR. The NMR experiment only had a single sample measured. The amount of ammonia is the total measured in the electrolyte and water trap, while the concentration is only the electrolyte. The reported energy efficiency does not account for the increase in pressure for any of the experiments.

Sample name	FE (%)	Charge (C)	NH_3 (μg)	NH_3 Conc. (p.p.m.)	Vol. (mL)	Energy efficiency (%)
Constant 1 (IP)	5.1 ± 0.1	73.2	219 ± 6	7.6 ± 0.2	28.7	0.7 ± 0.1
Constant 2 (IP)	4.9 ± 0.3	70.0	201 ± 11	6.5 ± 0.4	30.8	0.5 ± 0.1
Constant 3 (IP)	3.5 ± 0.3	72.1	147 ± 10	5.0 ± 0.3	29.6	0.5 ± 0.1
Cycling 1 (IP)	13.5 ± 0.8	100.0	793 ± 49	17.1 ± 1.9	25.6	2.2 ± 0.1
Cycling 2 (IP)	13.9 ± 1.2	100.0	815 ± 68	28.0 ± 2.6	26.3	2.6 ± 0.2
Cycling 3 (IP)	12.1 ± 0.7	100.0	711 ± 39	22.2 ± 1.4	27.7	2.2 ± 0.1

Table S2 All measured values for each indophenol experiment reported at 1 bar N_2 with 1 % EtOH. The mean and standard deviation stems from measured absorbance of 3 electrolyte samples from each measurement. Sample designated with numbers are repeated measurements under the same conditions. The amount of ammonia is the total measured in the electrolyte and water trap, while the concentration is only the electrolyte. The reported energy efficiency does not account for the increase in pressure for any of the experiments.

Sample name	FE (%)	Charge (C)	NH_3 (μg)	NH_3 Conc. (p.p.m.)	Vol. (mL)	Energy efficiency (%)
Constant 1 (IP)	24.9 ± 0.4	12.8	191 ± 3	6.4 ± 0.1	30.1	3.1 ± 0.1
Constant 2 (IP)	25.1 ± 2.2	75.6	1116 ± 97	38.6 ± 3.4	28.7	3.8 ± 0.3
Constant 3 (IP)	24.2 ± 1.2	75.0	1067 ± 51	36.2 ± 1.7	29.5	2.3 ± 0.1
Cycling 1 (IP)	43.5 ± 2.2	100.0	2562 ± 132	68.5 ± 4.5	29.4	7.1 ± 0.4
Cycling 2 (IP)	39.8 ± 0.8	100.0	2339 ± 49	52.3 ± 1.6	29.9	6.5 ± 0.2
Cycling 3 (IP)	39.4 ± 2.8	100.0	2316 ± 164	70.70 ± 5.5	29.7	7.3 ± 0.5

Table S3 All measured values for each indophenol experiment reported at 20 bar N_2 with 1 % EtOH. The mean and standard deviation stems from measured absorbance of 3 electrolyte samples from each measurement. Sample designated with numbers are repeated measurements under the same conditions. The reported energy efficiency does not account for the increase in pressure for any of the experiments.

Sample name	EtOH (vol.%)	FE (%)	Charge (C)	NH_3 (μg)	NH_3 Conc. (p.p.m.)	Vol. (mL)	Energy efficiency (%)
Cycling low EtOH (IP)	0.75	36.1 ± 1.5	100.0	2123 ± 90	54.8 ± 3.1	28.8	6.1 ± 0.3
Cycling high EtOH (IP)	1.50	33.8 ± 0.4	100.0	1986 ± 21	43.3 ± 0.6	35.0	5.6 ± 0.1
Cycling long (IP)	2.00	33.1 ± 1.0	178.3	3470 ± 104	110.9 ± 3.5	29.5	5.3 ± 0.2
Ar blank (IP)	1.00		100.7	15 ± 2	0.5 ± 0.1	28.0	
Ar blank (NMR)	1.00		100.7	12	0.4	28.0	
N_2 OCV (IP)	1.00			11 ± 1	0.4 ± 0.1	30.4	

Table S4 Measured values for indophenol experiment reported at 10 bar N_2 with variable EtOH concentrations, and data of blank and background measurements of 10 bar Ar with potential and 10 bar N_2 at OCP for 24 hours. The mean and standard deviation stems from measured absorbance of 3 electrolyte samples from each measurement. The amount of ammonia is the total measured in the electrolyte and water trap, while the concentration is only the electrolyte. The reported energy efficiency does not account for the increase in pressure for any of the experiments.

Figure S1 *Left*) Picture of Mo electrode after short constant deposition experiment at -2 mA/cm^2 passing 22 C. *Right*) Picture of Mo electrode after long-term cyclic stabilization experiment over 125 hours, passing of 180 C. Visually, the electrode surface of the constant deposition experiment had big deposits of lithium species on the surface. These deposits lead to the instability in the system in Figure 1, as it slowly passivates the electrode. The surface of the Mo foil used for passing 180 C over 125 hours is visually much cleaner and smoother. This correlates well with the experiment being stable and reproducible over long periods, as the lithium immediately near the electrode surface is repeatedly reduced and reacted off in the cycling process. The increase in FE and energy efficiency during the cycling compared to constant deposition implies that ammonia is formed even during the resting periods, wherein no net external current flows. EDX, SEM, XRD, and XPS of the electrodes post-electrochemistry is shown in Figure S2-S10. The composition of Li species on the surface is heavily oxygen dominated, as the samples are exposed to air to do the ex-situ measurements. Ex-situ XRD shows that the cycling sample only had hydrated $LiClO_4$ on the surface, while XPS showed a little additional carbon, most likely from dried THF and EtOH, all of which are from the electrolyte. We did not rinse the samples, as the thick deposits seen on the constant deposition sample were not mechanically stable, and would have flaked off during rinsing. The constant deposition sample had the same hydrated $LiClO_4$ XRD peaks, but additionally also had LiOH and hydrated LiOH species, as well as an amorphous phase. The LiOH could either be formed on the surface while the electrode is submerged in electrolyte at some point during the experiment, or come from the thick Li species deposited on the surface, which becomes LiOH upon being exposed to air, as that is one of the stable oxidized lithium species (*5*). An amorphous species was observed on this sample, and as XPS shows significantly more carbon compared to the cycling, it is suspected that there is a build-up of a passivating solid-electrolyte interface layer, which would be consistent with having an amorphous carbon species on the surface.

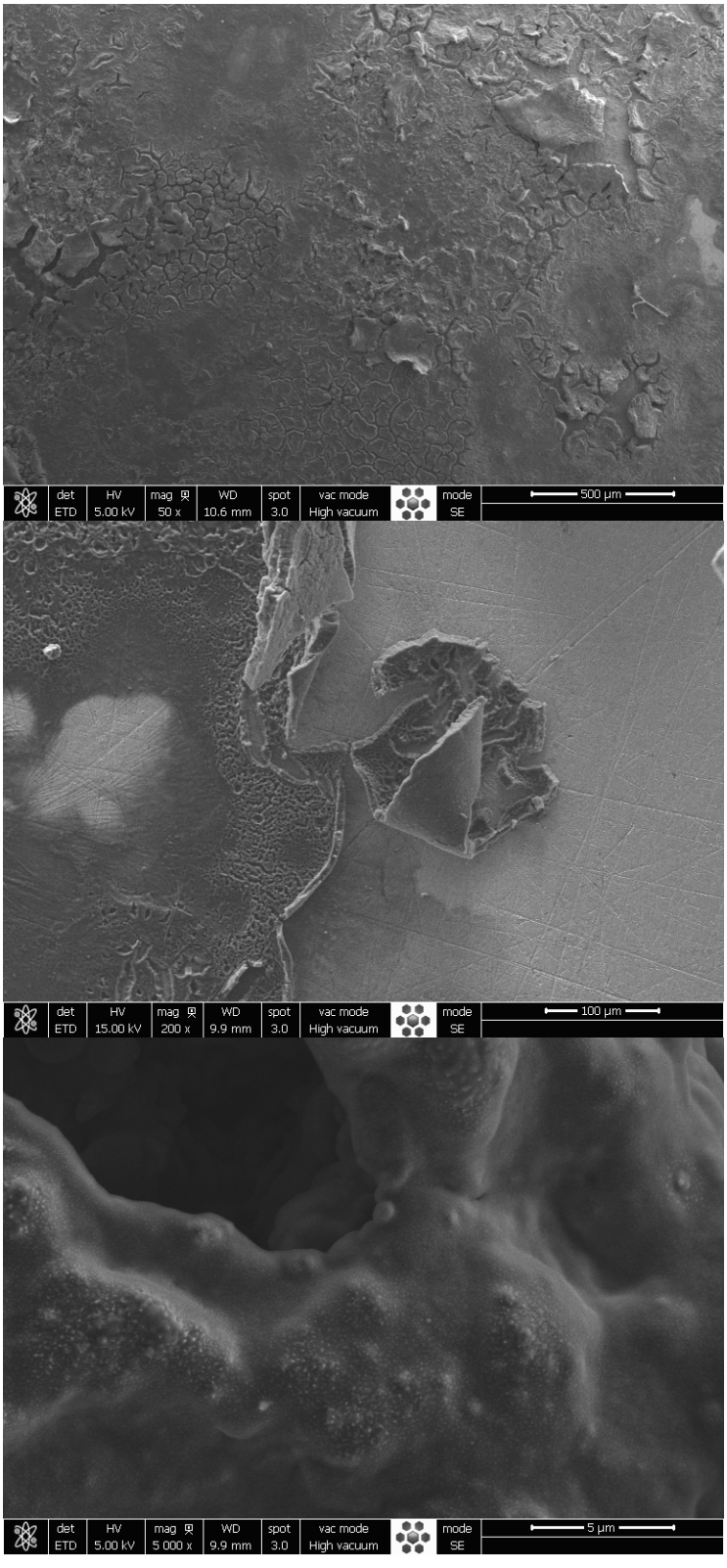

Figure S2 SEM images of the constant deposition sample. The surface is covered in a thick layer of lithium species, which upon being exposed to air has dried, and in some parts flaked off, exposing the Mo foil underneath.

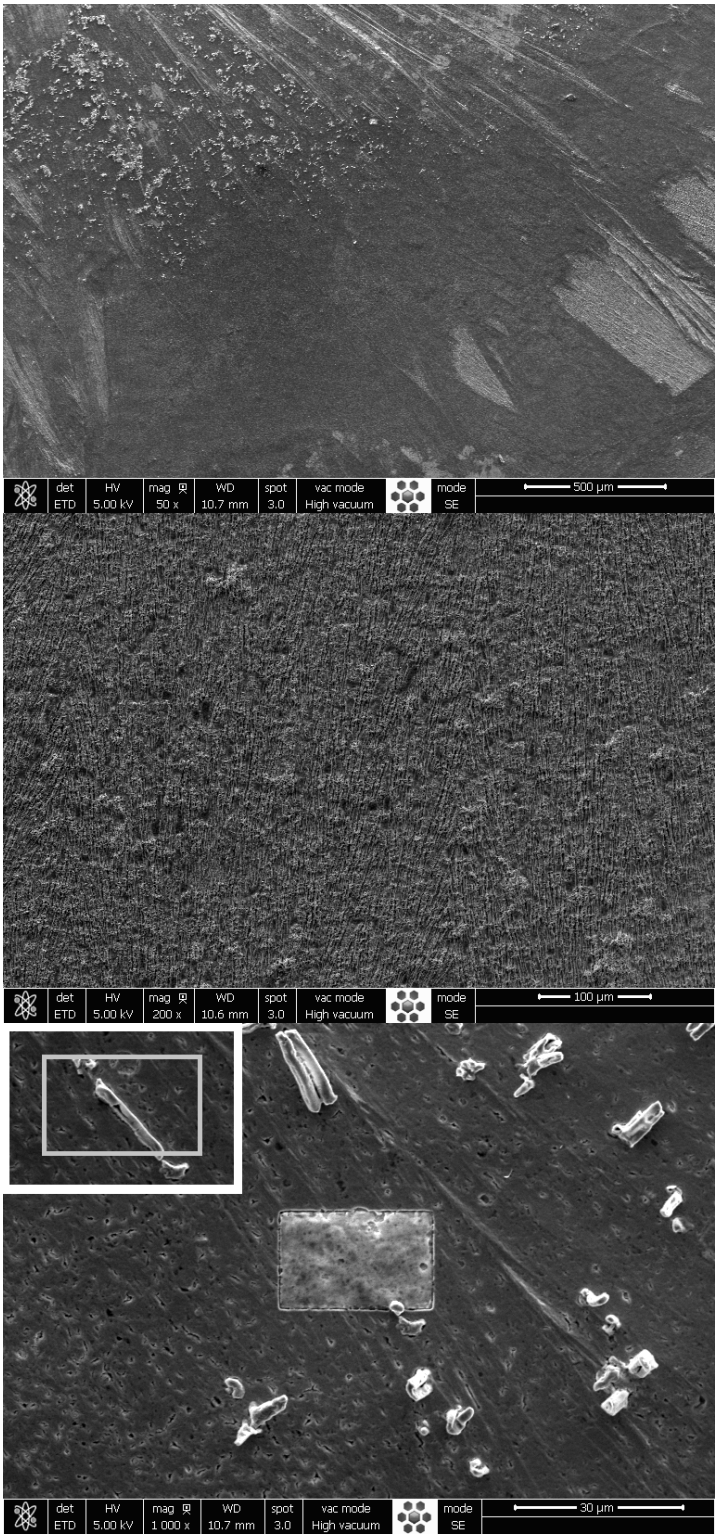

Figure S3 SEM images of the cycling sample. The sample was mostly uniform with a thin layer of deposition on top of the Mo foil; however one section (upper left corner) had whiskers of some lithium species, which disappeared upon focusing on them with the electron beam (see before image in inset).

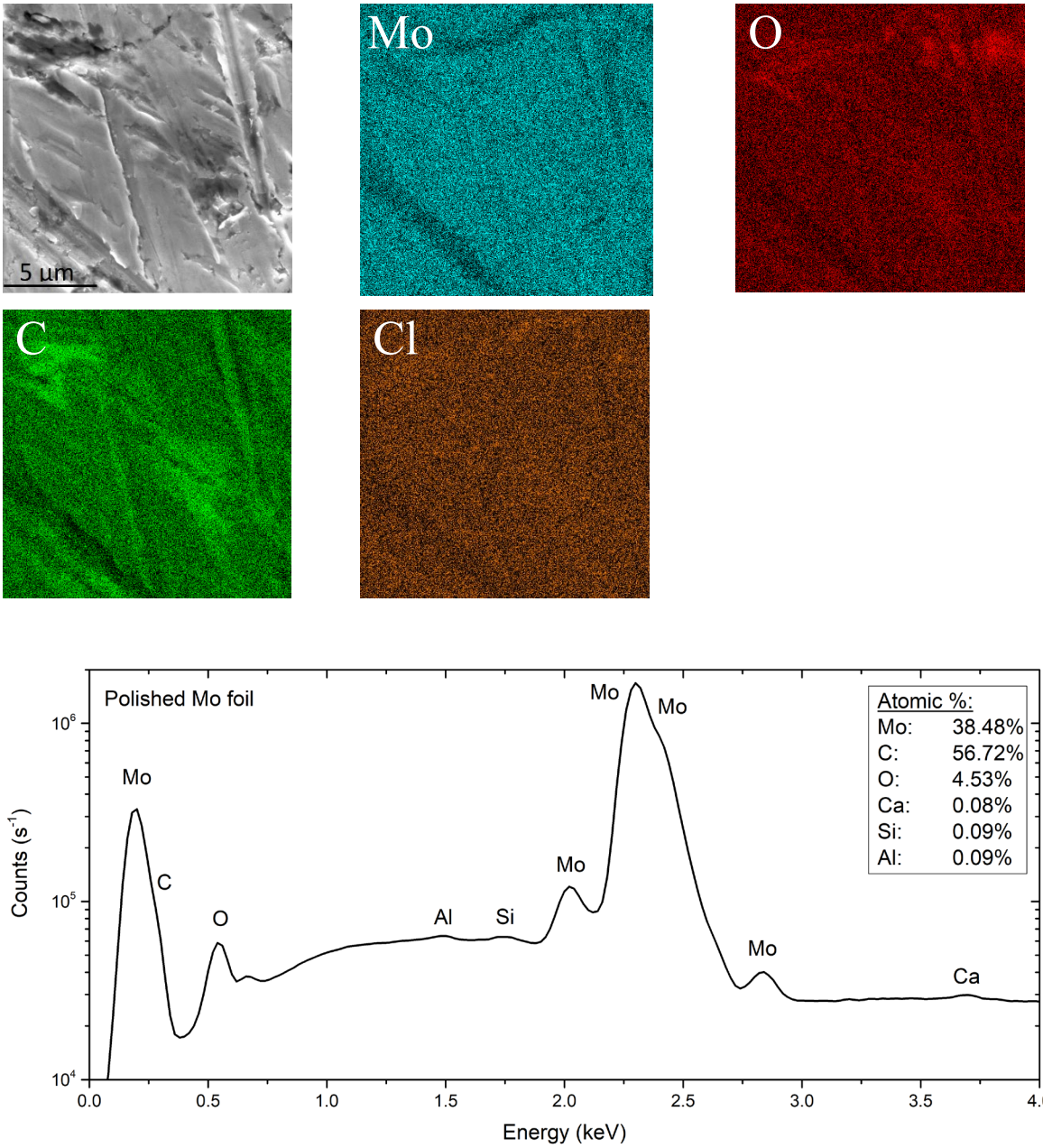

Figure S4 EDX data of Mo foil. The elemental mappings are auto-gamma corrected for lightning and visibility of colours. The small Si and Al peaks are respectively from the detector and sample stub, and we do not see them in XPS. We have a small amount of Ca contamination in the Mo foil, also observed with XPS, which is not seen in the Li covered samples (note the logarithmic y-axis to see the Ca peak). There are no peaks beyond 4.0 keV, so the remainder of the spectrum is not shown.

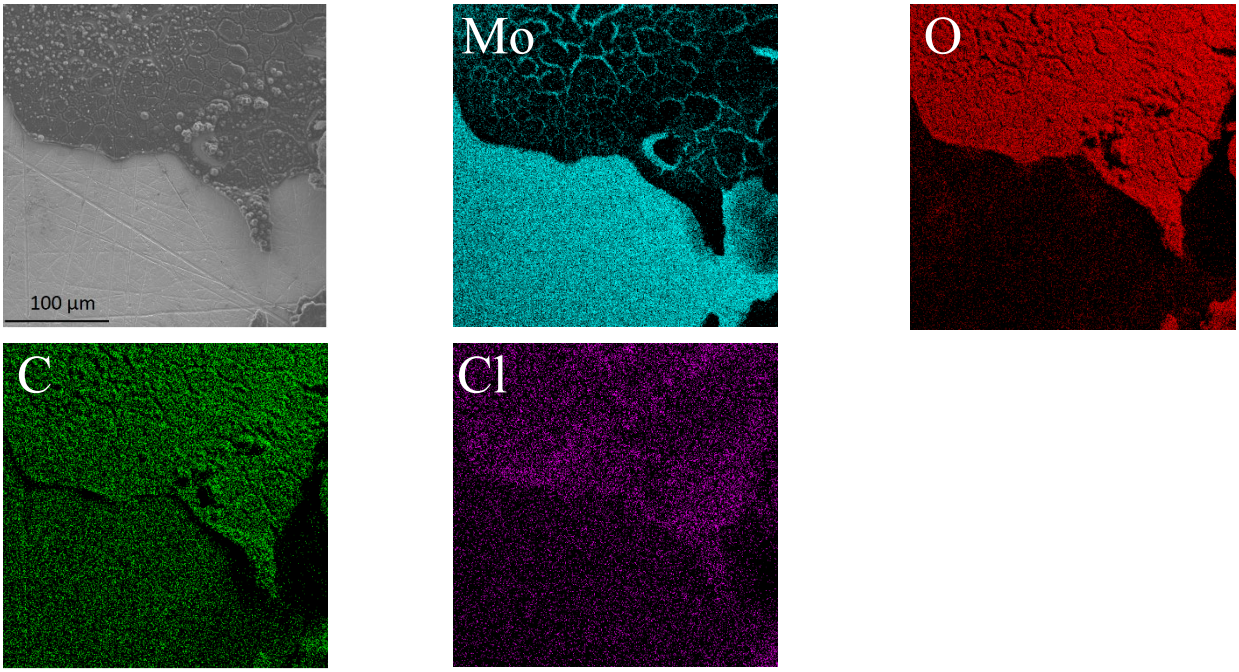

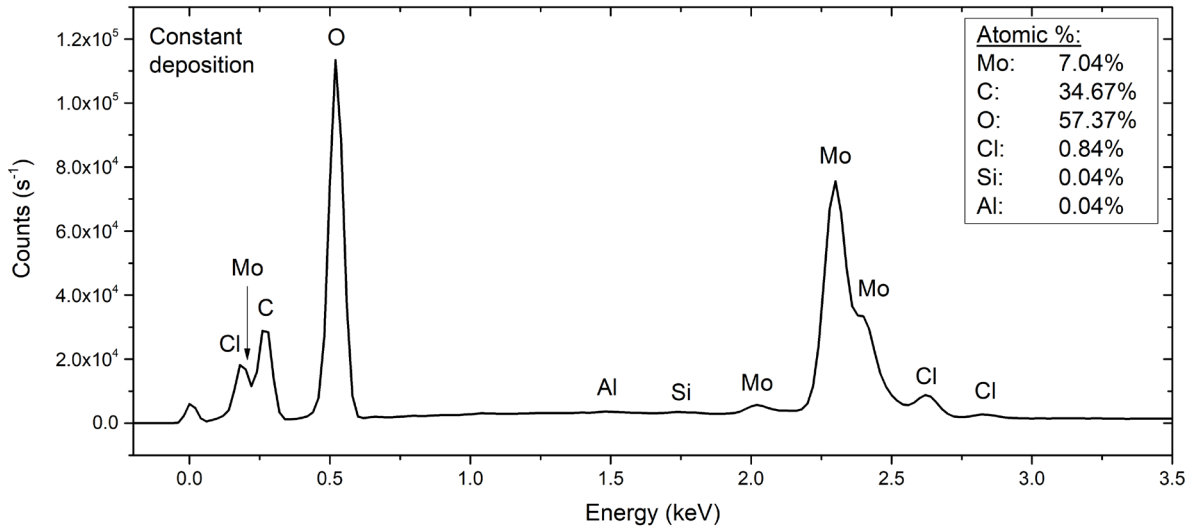

Figure S5 EDX data of constant current deposition sample. The elemental mappings are auto-gamma corrected for lightning and visibility of colours. The small Si and Al peaks are respectively from the detector and sample stub, as we do not see them in XPS. There are no peaks beyond 3.5 keV, so the remainder of the spectrum is not shown.

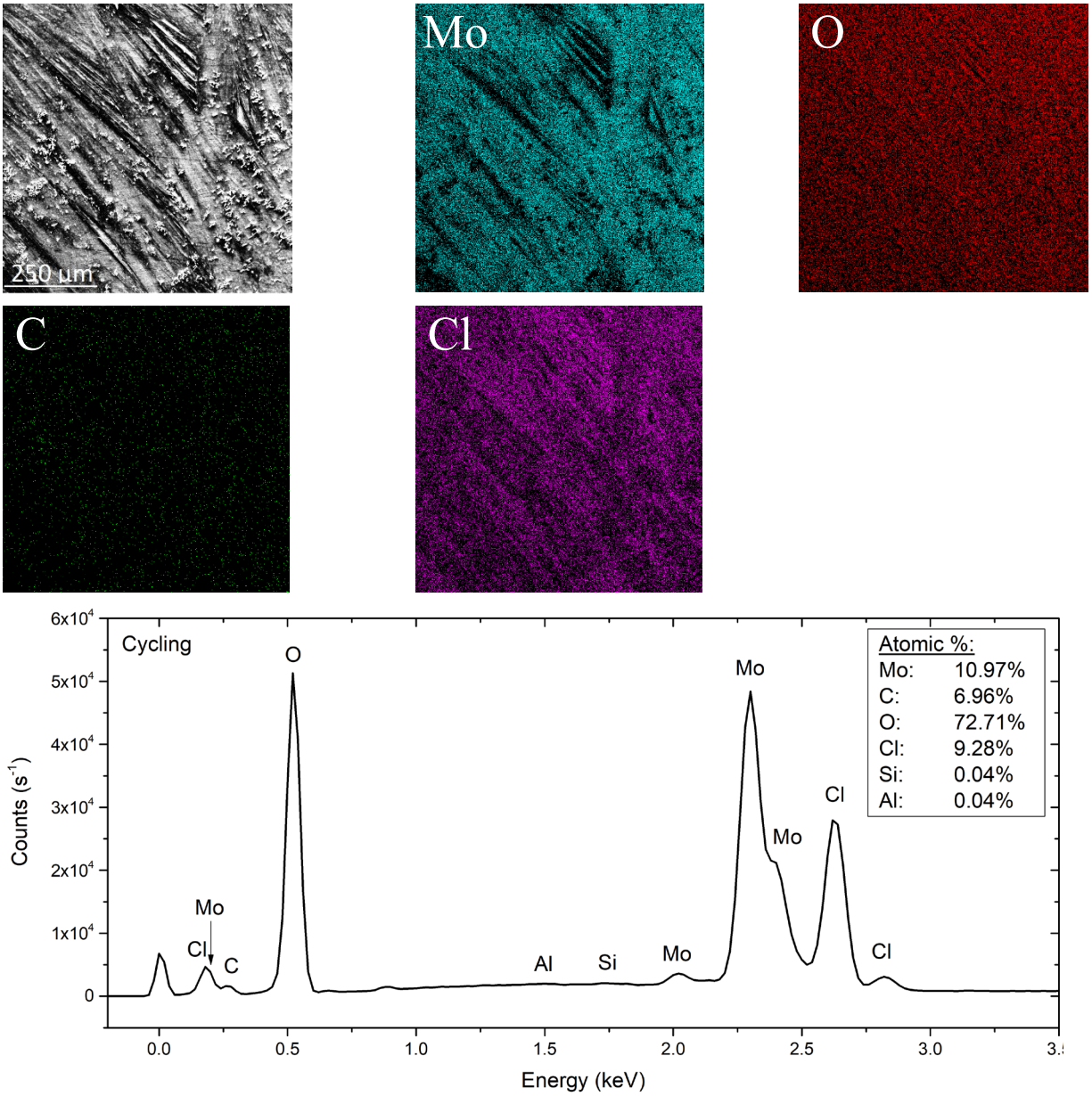

Figure S6 EDX data of 100 C cycling sample. The elemental mappings are auto-gamma corrected for lightning and visibility of colours. The small Si and Al peaks are respectively from the detector and sample stub, as we do not see them in XPS. There are no peaks beyond 3.5 keV, so the remainder of the spectrum is not shown.

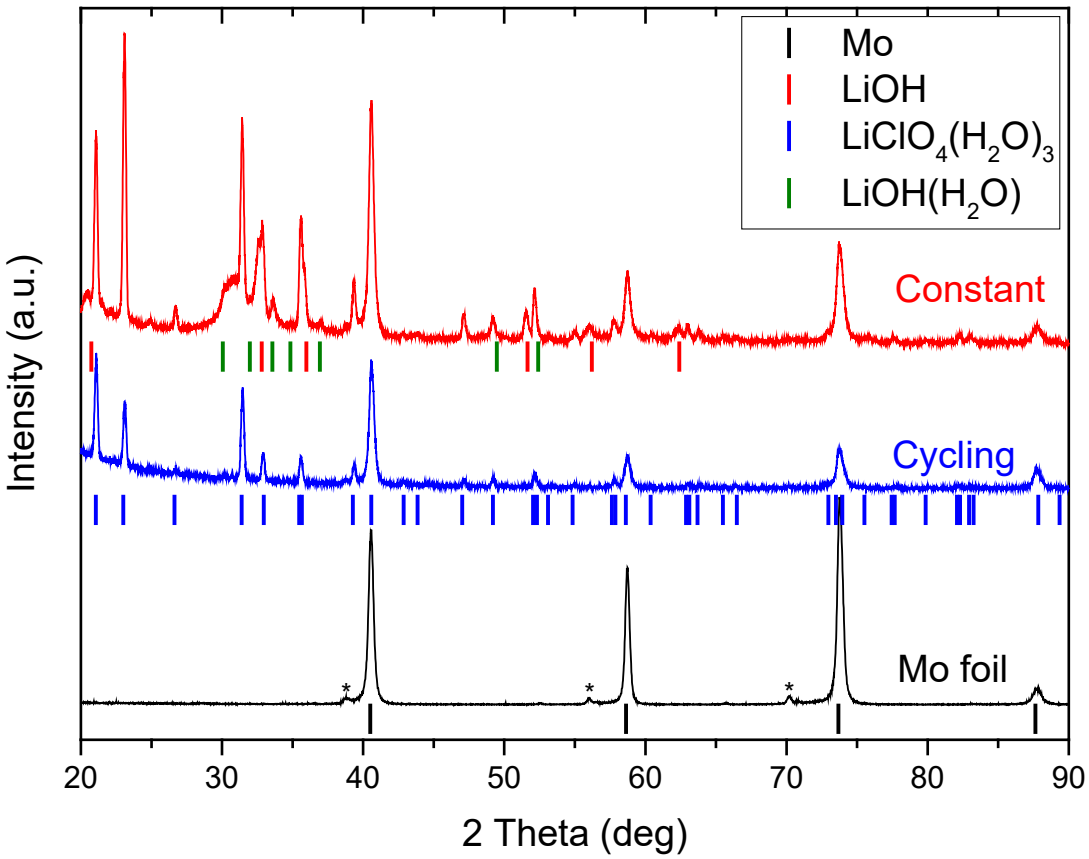

Figure S7 GI-XRD spectrum of polished Mo (ICSD:52267) foil, cycling sample, and constant current sample. The extra peaks denoted with * on the Mo foil are beta lines from the main peaks. These extra peaks are not visible in the electrochemistry samples, due to reduced intensity of the substrate from the GI angle. The samples were not rinsed, as the thick deposition of lithium species on the constant current sample are not mechanically well attached. The cycling sample has hydrated lithium perchlorate (ICSD:26737) on the surface, which mainly stems from the dried electrolyte exposed to air. The constant current deposition sample appears to have an amorphous phase, and some extra peaks besides the lithium perchlorate. These peaks are due to the thick deposition of Li on the sample, which is exposed to air to do ex-situ measurements, subsequently leading the lithium hydroxide (ICSD:26892) and hydrated lithium hydroxide (ICSD:35155) species on the surface to become oxidized.

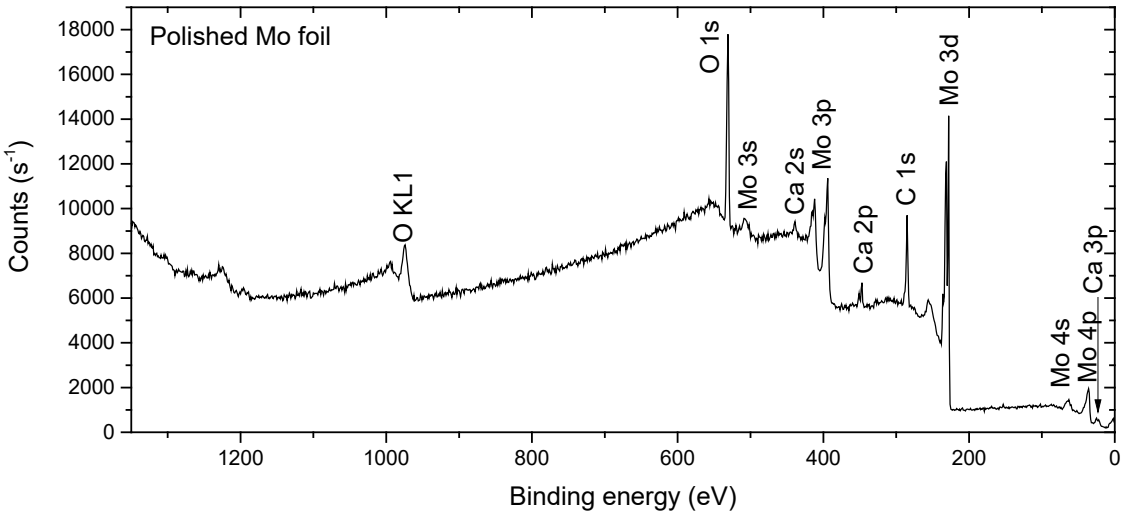

Figure S8 Representative XPS spectrum of the polished Mo foil. Using fitting of individual peak scans, the mean and standard deviation of the atomic percentage measured at 3 separate spots is given as: Mo: 15.4 ± 1.3 %, O: 38.6 ± 1.3 %, C: 43.4 ± 0.8 %, Ca: 2.3 ± 1.0 % and Na: 0.6 ± 0.5 %. There is a small calcium contamination in our Mo foil, which was also seen in EDX spectra, as well as very little sodium, which was only visible in two spots, and not at all in EDX.

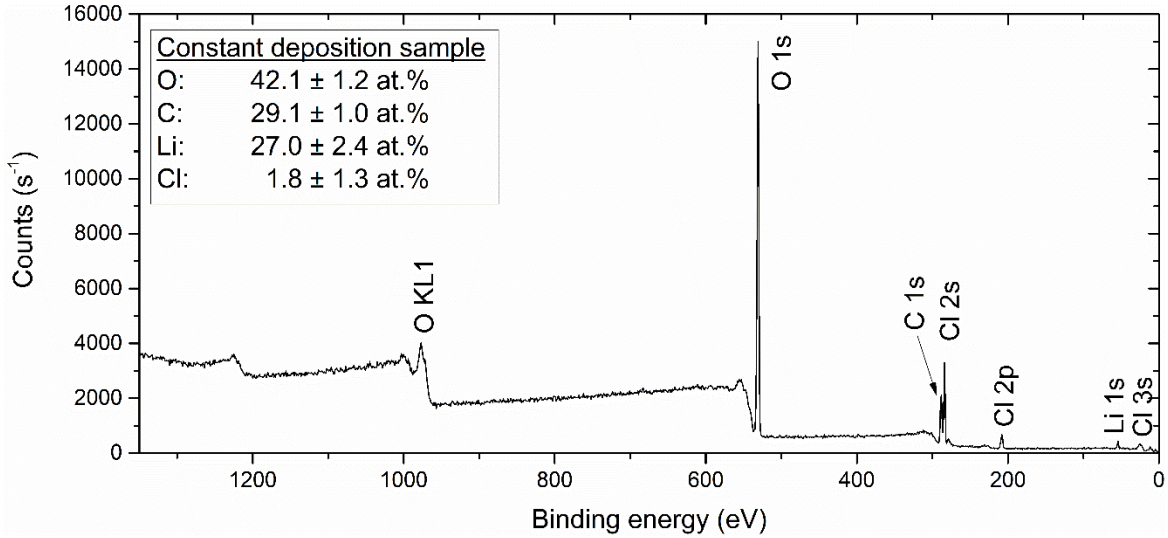

Figure S9 Representative XPS spectrum of the constant sample. Using fitting of individual peak scans, the mean and standard deviation of the atomic percentage measured at 3 separate spots is given as: O: 42.1 ± 1.2 %, Li: 27.0 ± 2.4 %, Cl: 1.8 ± 1.3 %, and C: 29.1 ± 1.0 %.

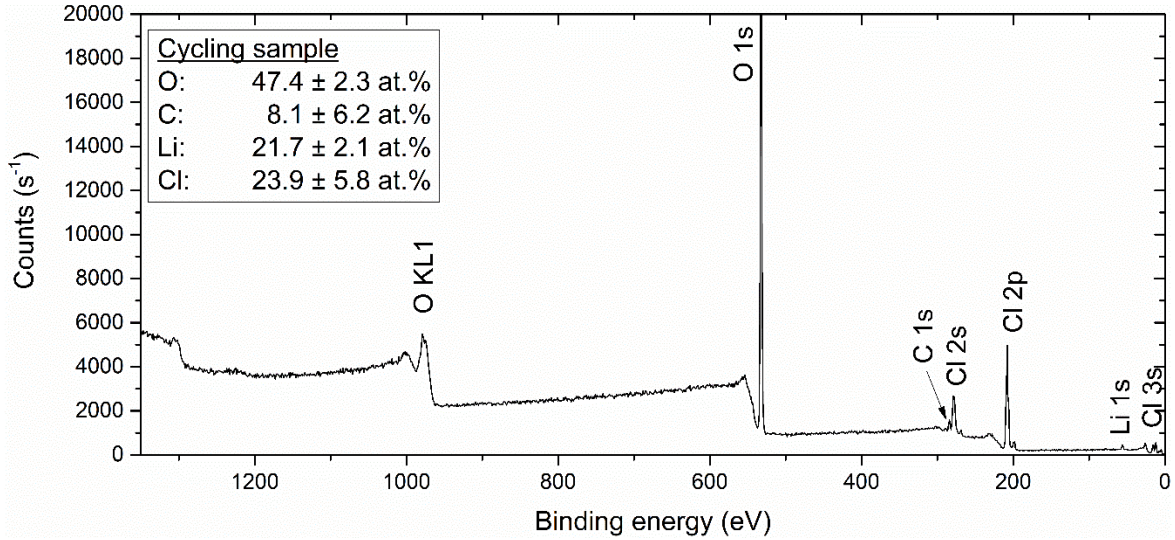

Figure S10 Representative XPS spectra of the cycling sample. Using fitting of individual peak scans, the mean and standard deviation of the atomic percentage measured at 3 separate spots is given as: O: 47.4 ± 2.3 %, Li: 21.7 ± 2.1 %, Cl: 23.9 ± 5.8 %, and C: 8.1 ± 6.2 %.

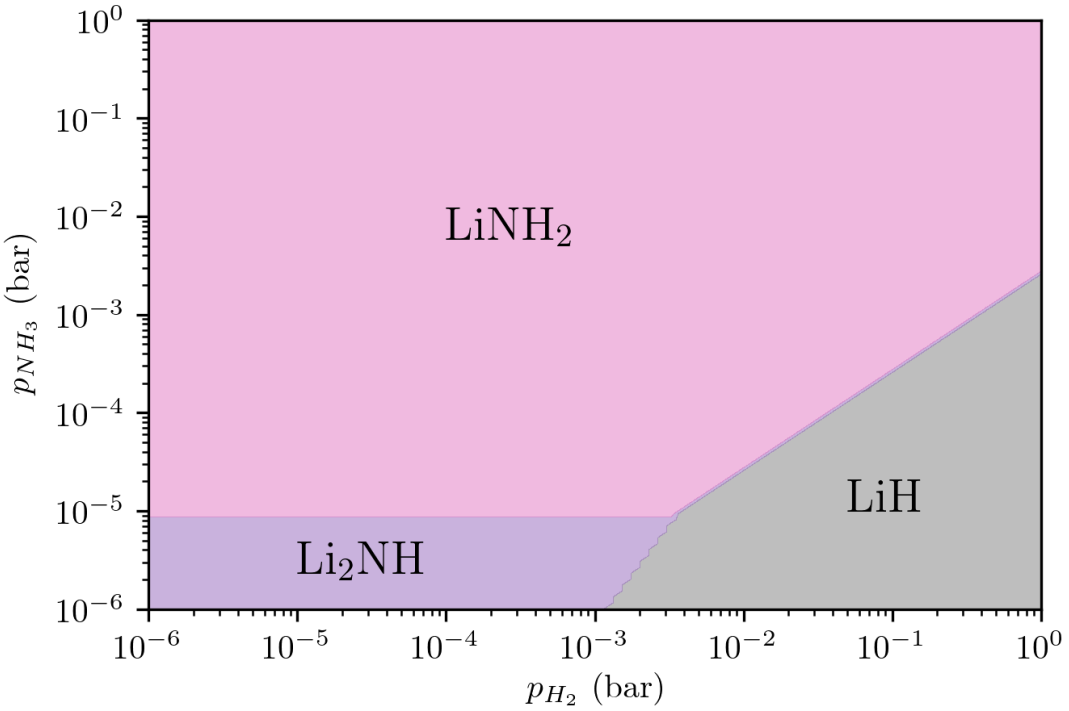

Figure S11 Two-dimensional phase diagram showing the most stable bulk phases of Li-N-H species using molecular hydrogen and ammonia as reference states for H and N, respectively.

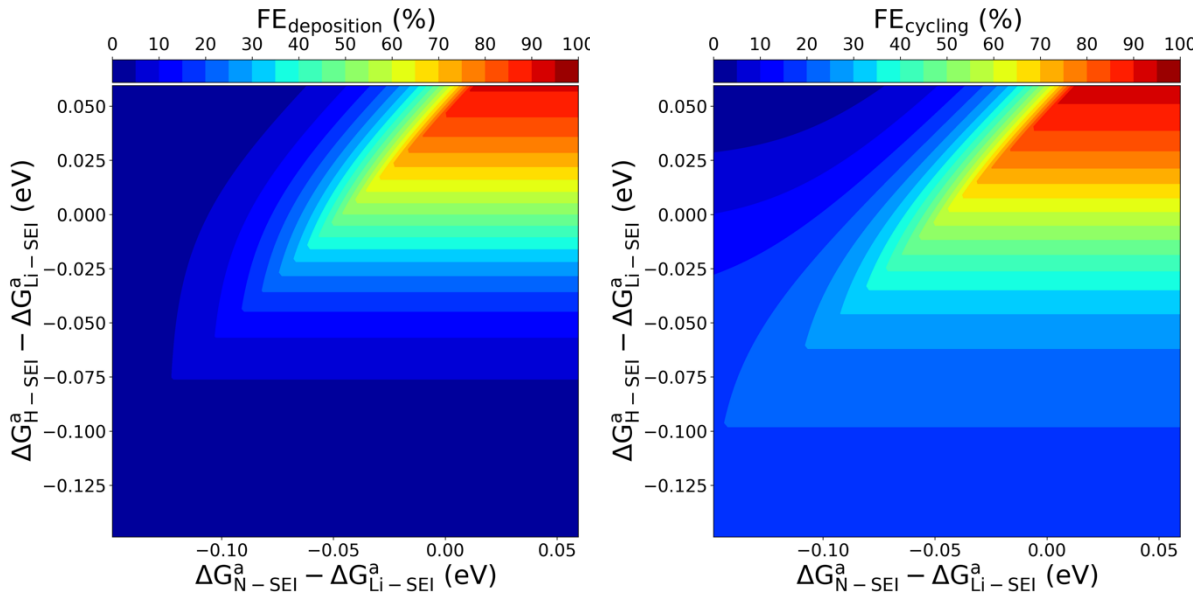

Figure S12: Heat maps of (a) Equation (6) and (b) Equation (8) for the faradaic efficiency during constant deposition and cycling, respectively. The axes are shown as the difference in diffusion barrier instead of ratio of rates, assuming a constant pre-factor for all three species. This illustrates how extremely small differences in diffusion barrier can lead to large differences in FE.

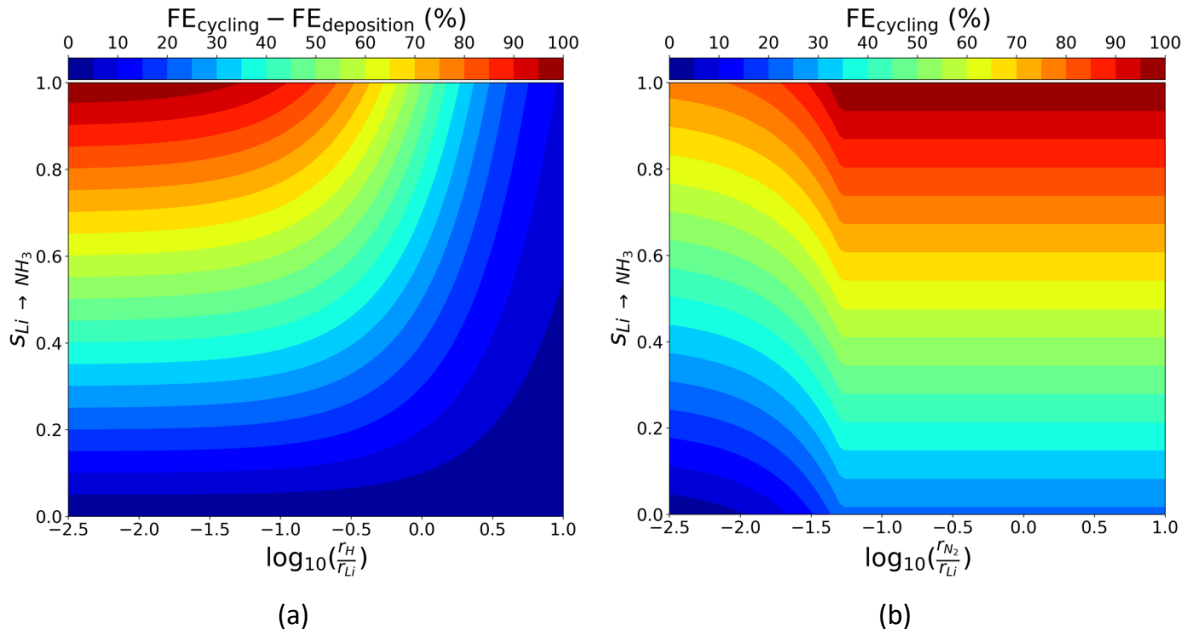

Figure S13: Heat maps showing (a) the difference in FE due to cycling and (b) the FE of cycling as a function of nitrogen and hydrogen rate ratios and the selectivity of lithium to ammonia recovery, $\boldsymbol{s_{Li \rightarrow NH_3}}$. (b) is plotted for a constant value of $\boldsymbol{r_H/r_{Li}}$=0.31, which corresponds to $\boldsymbol{C_{EtOH}}$=1 vol% from the fitted model parameters.

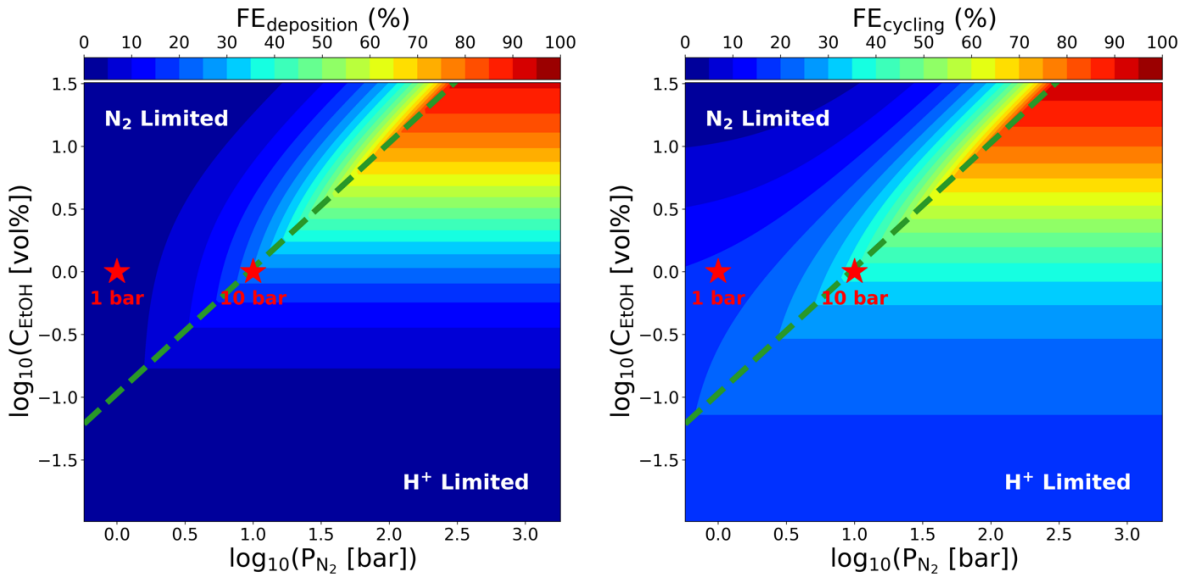

(a) (b)

Figure S14: *Heatmap of the predicted FE as a function of the ratio of nitrogen pressure (x-axis) and ethanol concentration (y-axis) diffusion rates. The left panel shows the FE during constant Li deposition (using Eq. (6)), while the right panel shows the FE during potential cycling (using Eq. (8)). In both cases, the green line indicates the boundary between regimes of N_2 transport limitations (upper left) and H^+ transport limitations (lower right). The stars have been specifically placed to show where our experimentally measured FE values at 1 and 10 bar would fall on this plot.*

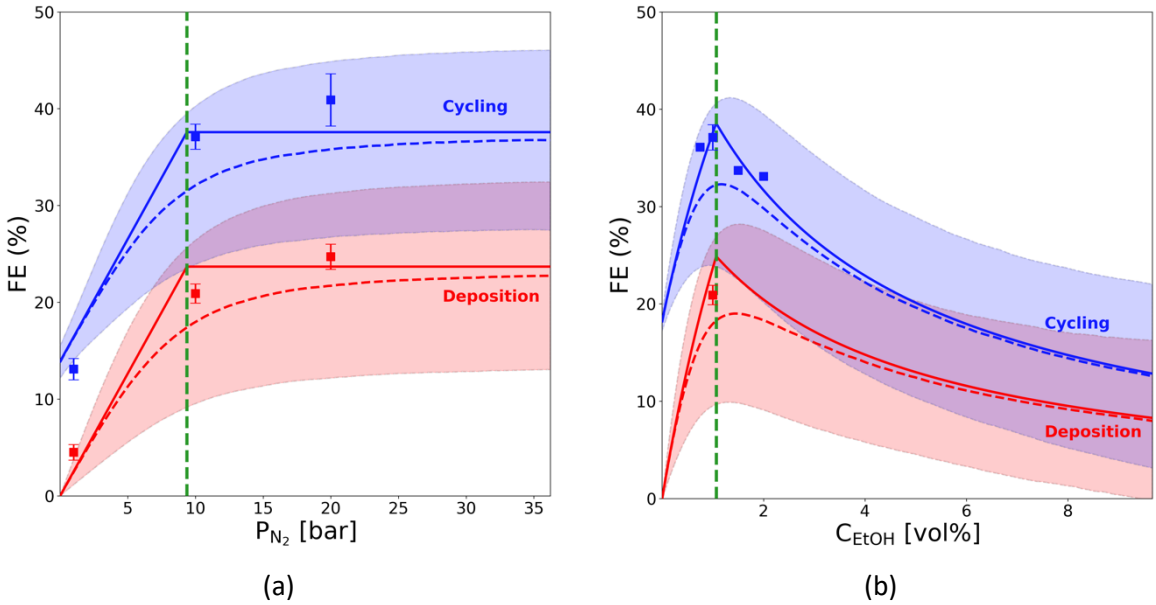

Figure S15: *Predicted FE as a function of the ratio of (a) nitrogen pressure and (b) proton to ethanol concentration. Red and blue lines show the FE during constant Li deposition and potential cycling respectively, while the dashed green line indicates the boundary between regimes of N_2 and H^+ transport limitations. The shaded region surrounding each curve illustrates the spread of FE as a result of ± 50% uncertainty in the ratio of diffusion rates for nitrogen and hydrogen. Panels (a) and (b) consider fixed values of $\boldsymbol{C_{EtOH}}$= 1 vol% and $\boldsymbol{P_{N_2}}$= 10 bar respectively. The experimental values are converted to ratios of diffusion rates using the conversion factors derived in the Kinetic Model Fitting section above. Error bars are calculated from 3 identical experiments (n=3). Single measurements (n=1) are shown without error bars. Experimental data of constant deposition at 1 bar is from a previously published report (13).*